aerospace

MDPI

Article

Optimal Selection of Active Jet Parameters for a Ducted Tail Wing Aimed at Improving Aerodynamic Performance

Huayu Jia [1,2], Huilong Zheng [1,3,*], Hong Zhou [1,3] and Shunbo Huo [1,2]

[1] The Institute of Engineering Thermophysics, Chinese Academy of Sciences, Beijing 100190, China; jiahuayu@iet.cn (H.J.); zhouhong@iet.cn (H.Z.); huoshunbo@iet.cn (S.H.)
[2] University of Chinese Academy of Sciences, Beijing 100049, China
[3] National Key Laboratory of Science and Technology on Advanced Light-Duty Gas-Turbine, Beijing 100190, China
* Correspondence: huilongzheng_ucas@163.com

Abstract: The foldable tail of the box-type launch vehicle poses a risk of mechanical jamming during the launch process, which is not conducive to the smooth completion of the flight mission. The integrated nonfolding ducted tail proposed in this article can solve the problem of storing the tail in the launch box. Moreover, traditional mechanical control surfaces have been eliminated, and active jet control has been adopted to control the pitch direction of the flight attitude, which can improve the structural reliability of the tail wing. By studying the effects of parameters such as momentum coefficient, jet hole position, jet hole height, and jet angle on improving the aerodynamic performance of ducted tail wing, relatively good jet parameters are selected. Research has found that compared with jet hole height and jet angle, momentum coefficient and jet hole position are more effective in improving the aerodynamic performance of ducted tail wings. Under a trailing edge jet, a relatively good jet condition occurs when the jet hole height is equal to0.25% of the aerodynamic chord length, and the jet angle is equal to 0°. At this time, with the increase of the jet momentum coefficient, the effect of increasing the lift of the ducted tail wing is the best. Finally, a comparative analysis is conducted on the lift and drag characteristics between the ducted tail wing and traditional tail wing, and it is found that the ducted tail wing can generate lift at a 0° attack angle and will not stall in the high attack angle range of 12°~22°, with broad application prospects.

Keywords: ducted tail wing; flow control; active jet; aerodynamic performance

Citation: Jia, H.; Zheng, H.; Zhou, H.; Huo, S. Optimal Selection of Active Jet Parameters for a Ducted Tail Wing Aimed at Improving Aerodynamic Performance. *Aerospace* **2024**, *11*, 851. https://doi.org/10.3390/aerospace11100851

Academic Editor: Christian Breitsamter

Received: 19 August 2024
Revised: 3 October 2024
Accepted: 14 October 2024
Published: 15 October 2024

1. Introduction

The traditional mechanical control surface changes the curvature of the wing by deflecting the wing surface, thereby altering the pressure values on the upper and lower surfaces of the wing, generating sufficient force and momentum to control the aircraft's flight attitude [1,2]. However, traditional control surface deflection destroys the aerodynamic stealth shape of the aircraft, increases structural weight, and is prone to mechanical jamming during the deflection process, posing certain safety hazards [3,4]. The emergence of active jet technology has greatly improved this situation. By intervening in the airflow distribution on the wing surface through an active jet without the need for rudder deflection, the required aerodynamic force and momentum for flight control can be obtained.

The academic community has conducted extensive research on active jet technology in improving aircraft performance and flight control. Englar [5] summarized the experimental progress of circulation control and aerodynamic lift systems and was the first to propose that circulation control technology can generate forces and momentum to control aircraft motion. A large amount of research on circulation control technology in this area has been carried out since then. Wood [6] found through further research that changing the magnitude of the jet momentum coefficient may cause significant changes in the lift coefficient. In 2010, BAE Systems collaborated with several universities in the UK to develop the DEMON unmanned

verification aircraft, which replaced traditional mechanical control surfaces with jet control surfaces and used active jet technology for flight control verification [7]. Hoholis [8] applied the circulation control device to the virtual control surface of unmanned aerial vehicles and found that, compared with traditional mechanical control surfaces, the circulation control device can generate control momentum for rolling flight at low attack angles. However, the circulation control device will completely fail at high attack angles, posing a serious threat to safe flight. Xu [9,10] takes wind turbine wings as the research object and optimizes the circulation control parameters through a particle swarm optimization algorithm to increase the performance of the wing shape. Fu [11] compared and studied the similarities and differences between traditional flaps and blowing jet control through numerical simulation. The results showed that different jet momentum coefficients can represent different deflection angles of flaps. However, the momentum coefficient of the jet is nonlinearly correlated with the deflection angle of the flaps. Visser [12] optimized the position and parameters of the jet at the leading edge of a flying wing layout aircraft and found that arranging tangential jet holes along the spanwise direction is most beneficial for aircraft attitude control. Amitay [13] installed synthetic jet control devices on the wings of a stingray layout aircraft and studied the effect of synthetic jet devices on the aerodynamic performance of the aircraft in three directions. The results indicate that the synthetic jet device can effectively capture the large vortex structures generated by separation and delayed separation through pulse modulation technology. Smith [14] arranged an array of synthetic jet devices on the wing surface of a flying wing layout aircraft and found that by applying synthetic jet control technology, the lift of the aircraft can be increased by up to 15% and the drag can be reduced by up to 10% at high angles of attack. The external incentive effect is superior to the internal incentive effect. Linear control of the aircraft can be achieved by adjusting the intensity of jet excitation and the number of jet holes. Englar [15] installed a stable jet device on a certain wing and found that under steady jet conditions, the wing has the advantage of generating positive lift at negative attack angles and increasing stall angles of attack. Jones [16,17] studied the control effects of pulsed and stable jets. The research results indicate that for the same magnitude of lift coefficient increase, the energy required for pulsed jets is lower than that required for steady jets. Liu [18] studied the effect of the square wave pulse jet and stable jet on lift increment. Under constant mass flow rate and jet momentum coefficient, a high-frequency pulse jet is more effective in improving lift than a steady jet. Feng [19] proposed a plasma circulation control method and constructed a nonrudder jet control model for the NACA0012 wing. The plasma circulation was used to create a stable pressure difference at the trailing edge of the wing, resulting in a virtual flap control effect. Pititat and Rajnish [20] introduced the large eddy simulation (LES) algorithm in numerical simulations to investigate the effect of the circulation formed by synthetic jets on the aerodynamic performance of the NACA0015 airfoil. The study found that synthetic jets contribute to a linear increase in lift at low momentum coefficients.

The above research indicates that active jet technology has the potential to replace traditional mechanical control surfaces and is beneficial for increasing lift and reducing drag of aircraft. The integrated nonfolding ducted tail proposed in this article can solve the problem of storing the tail in the launch box. Moreover, traditional mechanical control surfaces have been eliminated, and active jet control has been adopted to control the pitch direction of the flight attitude, which can improve the structural reliability of the tail wing. At present, there is limited research available on the impact of the combination of ducted tail wings and active jet control technology on the aerodynamic performance of aircraft. This article has made the following contributions to improving the aerodynamic performance of active jet ducted tail wings:

(1) By studying the effects of parameters such as momentum coefficient, jet hole position, jet hole height, and jet angle on improving the aerodynamic performance of the ducted tail wing, we found that compared with jet hole height and jet angle, momentum

coefficient and jet hole position are more effective on improving the aerodynamic performance of the ducted tail wing.

(2) Under a trailing edge jet, the relatively good jet condition occurs when the jet hole height is equal to 0.25% of the aerodynamic chord length, and the jet angle is equal to 0°. At this time, with the increase of the jet momentum coefficient, the effect of increasing lift of the ducted tail wing is the best.

(3) Finally, a comparative analysis is conducted on the lift and drag characteristics between the ducted tail wing and traditional tail wing, and it is found that the ducted tail wing can generate lift at 0° attack angle and will not stall in the high attack angle range of 12°~22°.

The main content of the remaining sections of this article is as follows. In Section 2, the research object and content of this article are elaborated. Section 3 elaborates on the selection of jet parameters and numerical simulation methods. Section 4 studies the effects of parameters such as momentum coefficient, jet hole position, jet hole height, and jet angle on improving the aerodynamic performance of ducted tail wings and analyzes the advantages of ducted tail wings compared with traditional ones. Finally, Section 5 summarizes the research work of this article and provides some conclusions.

2. Research Object

Box-type launch aircraft can be flexibly deployed in different scenarios and have broad military application prospects. In order to load the aircraft into the launch box, the main and tail wings of the box-type launch aircraft need to be folded, and after launch, the main and tail wings of the aircraft need to be unfolded, which can easily cause mechanical failure.

In order to reduce the adverse effects of folding the tail wing of a box-type launch aircraft, as shown in Figure 1, this paper proposes a ducted tail wing aircraft with the advantage of a compact structure that does not require folding in the launch box. Compared with the tail wing of traditional box-type launch aircraft, as shown in Figure 1a, the ducted tail wing proposed in this paper adopts a circular structure. The ducted tail wing does not need to be folded in the launch box and does not need to be unfolded after being launched from the box, which can improve the structural reliability of the tail wing. In addition, as shown in Figure 1b, the ducted tail wing eliminates the traditional mechanical deflection control surface and adds active jet devices to the ducted tail wing. By changing the jet parameters, the velocity and direction of the airflow passing through the tail wing are altered, thereby changing the lift coefficient of the tail wing and generating different control momentums.

Therefore, studying the influence of jet parameters on the aerodynamic performance of ducted tail fins is of great significance, and jet parameter modeling is a key step in this process. As shown in Figure 1c, due to the large aspect ratio flat fuselage of the ducted tail aircraft studied in this paper, and in order to simplify the problem, the aircraft's symmetrical plane was selected for parametric modeling in the modeling process of the ducted tail jet parameters. The NACA0012 airfoil is selected for the ducted tail wing, and the jet methods include leading edge jet and trailing edge jet. The influence of parameters such as momentum coefficient, jet hole position, jet hole height, and jet angle on the aerodynamic performance of the ducted tail wing are analyzed.

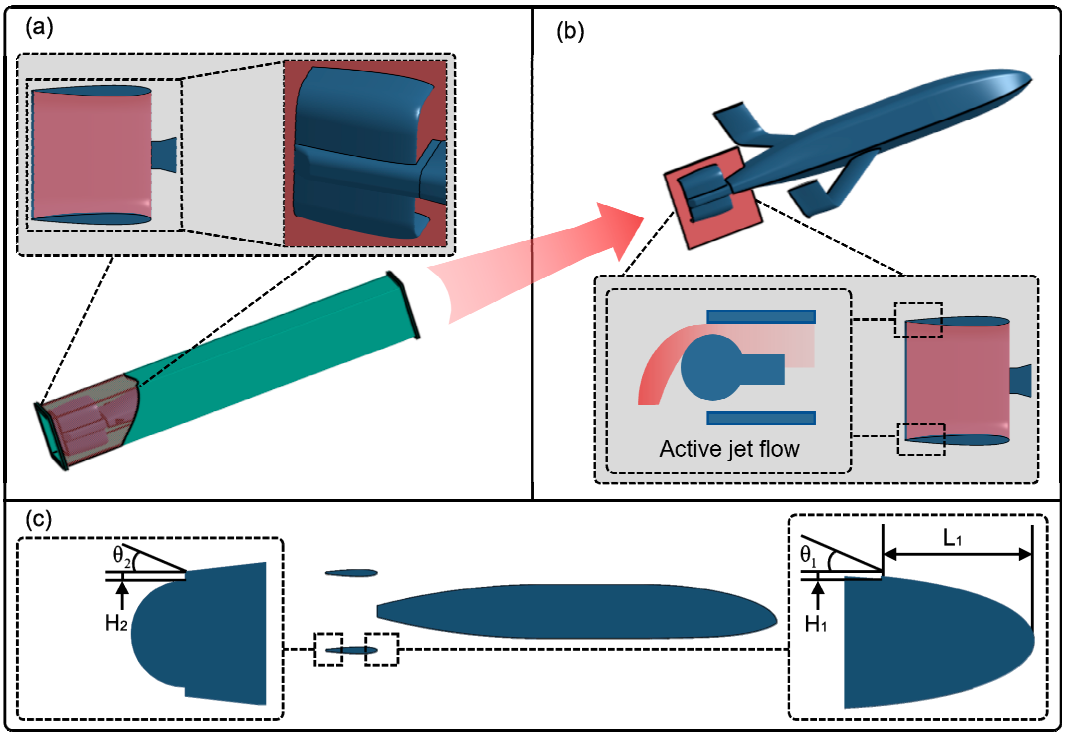

Figure 1. The advantages and parametric modeling of active jet ducted tail fins. (**a**) Compared with the traditional tail, the ducted tail in the launch box does not need to be folded; (**b**) during flight, the aircraft controls its flight attitude through an active jet ducted tail fin; (**c**) modeling jet parameters for ducted tail fins.

3. Jet Parameters and Numerical Simulation Methods

3.1. Selection of Active Jet Parameters

According to Figure 1c, the list of jet parameters is shown in Table 1.

Table 1. Jet parameter list.

Serial Number	Parameter	Values
1	C_μ	0.00/0.01/0.02/0.03/0.04
2	H_1	0.25%c
3	H_2	0.25%c/0.35%c/0.45%c
4	L_1	20%c/40%c/60%c/80%c/100%c
5	θ_1	0°/10°/20°/30°
6	θ_2	0°

Among them, C_μ is the momentum coefficient, H_1 and H_2 are the heights of the jet holes, L1 is the relative position of the jet hole (measured based on the leading edge of the tail wing), θ_1 and θ_2 are the jet angles, and the heights and lengths mentioned in this article are expressed as a percentage of the tail wing chord length c. Calculate the momentum coefficient using the following formula:

$$C_\mu = \frac{m_j v_j}{\frac{1}{2}\rho v_\infty^2 s}, \tag{1}$$

$$m_j = \rho v_j A_j, \tag{2}$$

In the formula, m_j is the mass flow rate, ρ and v_∞ are the density and velocity of air at local atmospheric pressure, v_j is the jet velocity, A_j is the jet area, s is the wing area, respectively.

3.2. Simulation Method and Computational Grid Independence

3.2.1. Simulation Method

This article uses commercial numerical simulation software Fluent 2022R1 for CFD calculations, using a rectangular computational domain, with the external flow field boundary condition being the far-field pressure, the jet inlet boundary condition being the velocity inlet, and the wall boundary condition being the nonslip boundary condition. The method of solving the Reynolds-averaged Navier–Stokes (RANS) equation is used for fluid computational analysis, and the second-order upwind and implicit approximate factorization methods are used for spatial and temporal two-dimensional discretization calculations. The turbulence model selected is the coupled shear stress transport (SST) turbulence model.

3.2.2. Grid Independence Verification

Due to the selection of the NACA0012 airfoil for the ducted tail wing and the large aspect ratio flat fuselage, the model formed by the combination of the tail fins and fuselage is very complex. In order to study the influence of jet parameters on the aerodynamic performance of the ducted tail wing, both computational efficiency and accuracy need to be considered during grid partitioning. Therefore, the research object is simplified to the symmetry plane of the fuselage and ducted tail. In order to compare with traditional tail fins, a horizontal tail fin composed of NACA0012 airfoil was selected as the research object, simplified as solving the aerodynamic performance of NACA0012 airfoil.

As shown in Figure 2, the computational efficiency and accuracy of numerical simulation are taken into account, as well as the aerodynamic performance comparison with the traditional horizontal tail formed by the NACA0012 airfoil. Therefore, two validation models, namely the ordinary NACA0012 tail and the jet ducted tail, are selected to construct unstructured grids with different densities. Grid independence verification and numerical simulation accuracy evaluation are carried out. In order to better capture flow details, the mesh has been locally densified in the tail area, nozzle, and front and rear edges of the wing. Due to differences in the encryption area and grid size settings, the number of grids varies. The number of grids in this article is shown in Table 2.

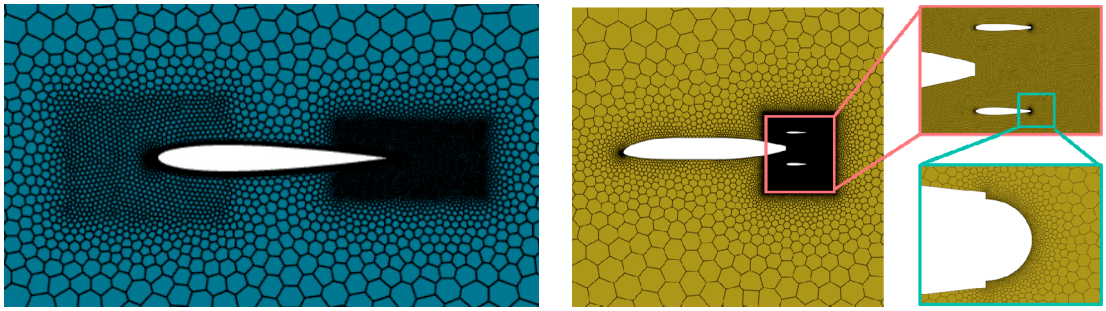

(**a**) (**b**)

Figure 2. Details of the grid. (**a**) Grid of ordinary tail wing; (**b**) grid of jet ducted tail wing.

Table 2. Number of grids with different accuracies.

Model	The Number of Sparse Grids	The Number of Medium Grids	The Number of Fine Grids
NACA0012 tail wing	$1.40 \times 10^5/2.10 \times 10^5$	$3.50 \times 10^5/4.70 \times 10^5$	6.80×10^5
Jet ducted tail wing	3.56×10^6	7.06×10^6	1.50×10^7

Verify that the numerical simulation method presented in this article is independent of the mesh division of the model. As shown in Figure 3, first verify the stability of the numerical simulation results of the ordinary NACA0012 tail wing under different grid numbers. It can be seen that the selected calculation conditions are height H = 0 m, reference

chord length $c_{ref} = 0.1$ m, Reynolds number Re $= 10^7$, and attack angle $\alpha = 10°$. As the number of calculation grids increases, especially when the number of grids is greater than or equal to 2.10×10^5, the lift coefficient of the ordinary tail wing stabilizes at 1.0034. In order to accurately evaluate the accuracy of the CFD calculation method in this article, the numerical simulation results of the traditional NACA0012 tail are compared with the wind tunnel experimental results in reference [21]. As shown in Figure 4, the maximum error between the simulated and wind tunnel experimental values of the traditional tail lift coefficient is less than 15%, and the direction of the lift curve is consistent. After evaluation, it can meet the calculation accuracy requirements of numerical simulation.

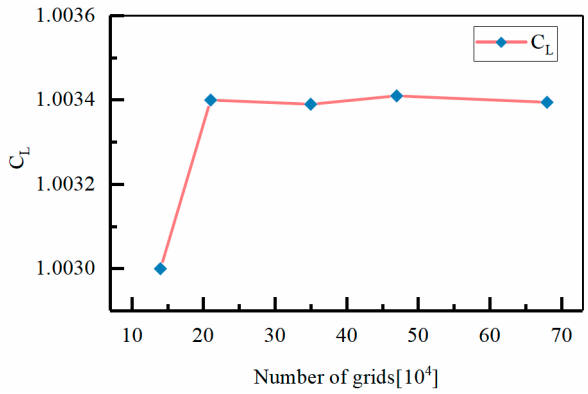

Figure 3. Verification of grid independence for the ordinary NACA0012 tail wing.

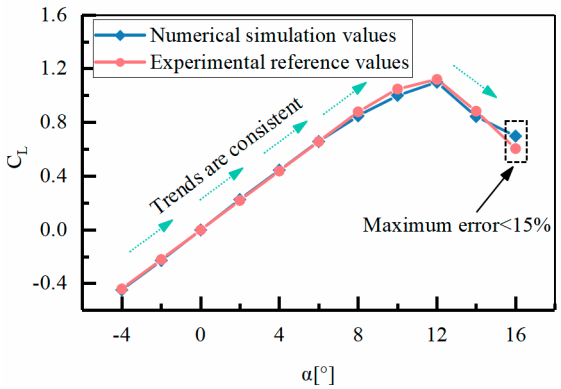

Figure 4. Verification of calculation accuracy for the ordinary NACA0012 tail wing.

Based on the above, the grid independence of the jet ducted tail is further verified. The selected operating conditions are jet momentum coefficient $C_\mu = 0$, altitude H = 0 m, inflow velocity 0.15 Ma, attack angle $\alpha = 18°$, reference area of ducted tail wing $S_d = 0.01$ m^2, aerodynamic chord length of ducted tail wing $c_{ref} = 0.1$ m, and reference span length 0.1 m. From Table 3, it can be seen that with the lift coefficient calculated under refined grid conditions as a reference, the calculation error of the lift coefficient for the other two sets of grids is less than 1.92%. Similarly, due to the difference in the number and density of boundary layer grids, the calculation error of the drag coefficient can reach up to 19.5%, but it can still meet the requirements of calculation accuracy. Therefore, this article chooses a model with a medium number of grids for subsequent numerical simulations.

Table 3. Grid independence of the jet ducted tail.

Aerodynamic Parameters	The Number of Sparse Grids	The Number of Medium Grids	The Number of Fine Grids
Lift coefficient	0.8791	0.8945	0.8963
Drag coefficient	0.1548	0.1887	0.1924

4. Result Analysis

4.1. The Improvement Effect of Momentum Coefficient on Aerodynamic Performance

Firstly, the improvement effect of the momentum coefficient on the aerodynamic performance of ducted tail wing is studied. The calculation state is selected as Reynolds number Re = 8.43 × 10^5, flow velocity Ma = 0.15, jet hole height H_1 = H_2 = 0.25%c, jet angle θ_1 = θ_2 = 0°, jet hole position L_1 = 20% or 100%, and jet momentum coefficient C_μ = 0.00/0.01/0.02/0.03/0.04.

As shown in Figure 5a, when the jet hole position L_1 = 100% c, the momentum coefficient of the jet gradually increases from C_μ = 0.00 to C_μ = 0.04. Due to the increased circulation intensity at the trailing edge of the ducted tail, the lift coefficient of the ducted tail is improved. As shown in Figure 5b, ΔC_L represents the increase in lift coefficient, within the angle of attack range of 0°~22°, with C_μ = 0.00 as the reference for the no jet state, the increase in lift coefficient C_L remains stable. At C_μ = 0.04, the average of ΔC_L is 0.403; When C_μ = 0.03, the average of ΔC_L is 0.329; When C_μ = 0.02, the average of ΔC_L is 0.262; When C_μ = 0.01, the average of ΔC_L is 0.191. When C_μ increases from 0.01 to 0.04, the average growth value of ΔC_L can reach 110%, indicating that the increase in momentum coefficient has a significant effect on the lift coefficient of the tail wing under the condition of a trailing edge jet. As shown in Figure 5c, when the jet hole position L_1 = 100%c, as the momentum coefficient increases, the energy disturbance injected into the trailing edge flow field per unit of time increases, increasing the drag coefficient C_D of the ducted tail wing. However, as shown in Figure 5d, the increase in drag coefficient is not significant within the range of 0°–8°. As the angle of attack continues to increase, the increase in drag coefficient gradually increases.

As shown in Figure 6a, when the jet hole position L_1 = 20%c, with the increase of momentum coefficient, the lift coefficient C_L of the ducted tail wing is also improved, but the improvement effect is not as good as that of the trailing edge jet. As shown in Figure 6b, within the angle of attack range of 0°–22°, the increase in lift coefficient C_L is relatively small when C_μ = 0.00 is used as the reference for the no jet state. At C_μ = 0.04, the average of ΔC_L is 0.116; When C_μ = 0.03, the average of ΔC_L is 0.056; When C_μ = 0.02, the average of ΔC_L is 0.008; When C_μ = 0.01, the average of ΔC_L is −0.029. Compared with the trailing edge jet (L_1 = 100%c), due to the higher airflow velocity at the leading edge of the tail wing, the airflow disturbance injected by the leading edge jet under the same conditions is smaller, resulting in a poorer lift coefficient enhancement effect. As shown in Figure 6c, when the jet hole position L_1 = 20%c, the drag coefficient C_D of the ducted tail does not change significantly with the increase of momentum coefficient. As shown in Figure 6d, within the range of 0°–20°, the excitation effect of the leading edge jet on the boundary layer airflow results in no significant increase in the drag coefficient.

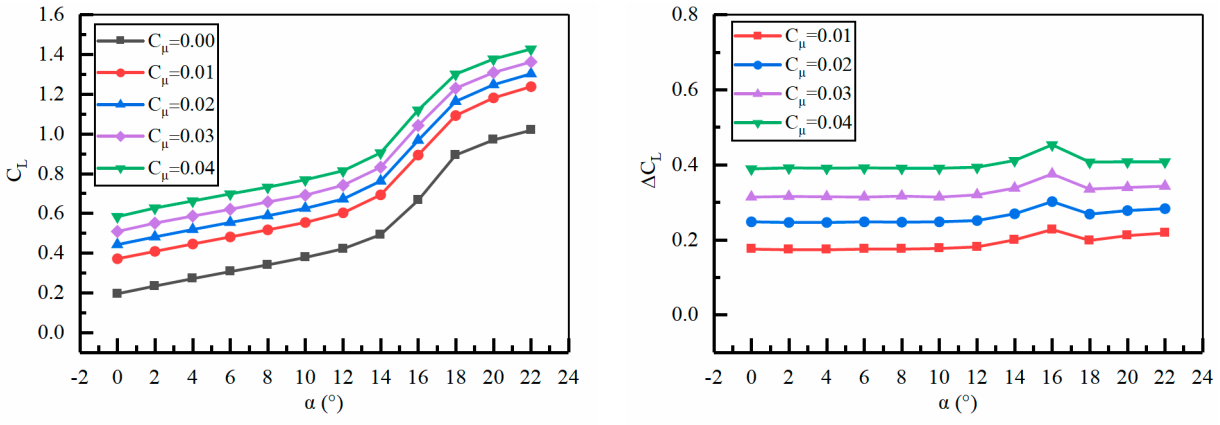

(**a**) (**b**)

Figure 5. *Cont.*

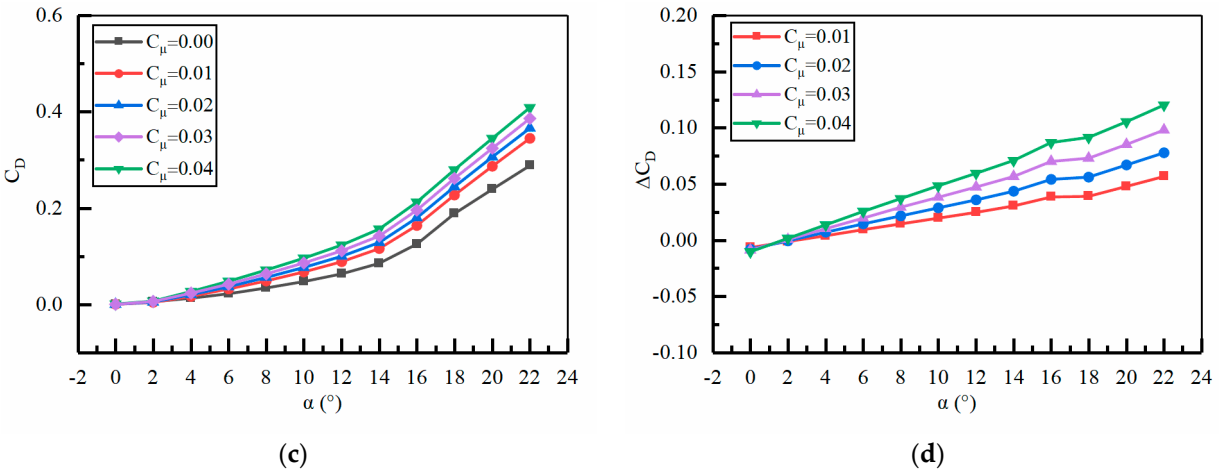

(**c**) (**d**)

Figure 5. The improvement effect of momentum coefficient on the aerodynamic performance under trailing edge jet conditions. (**a**) Lift coefficient; (**b**) growth value of lift coefficient; (**c**) drag coefficient; (**d**) growth value of drag coefficient.

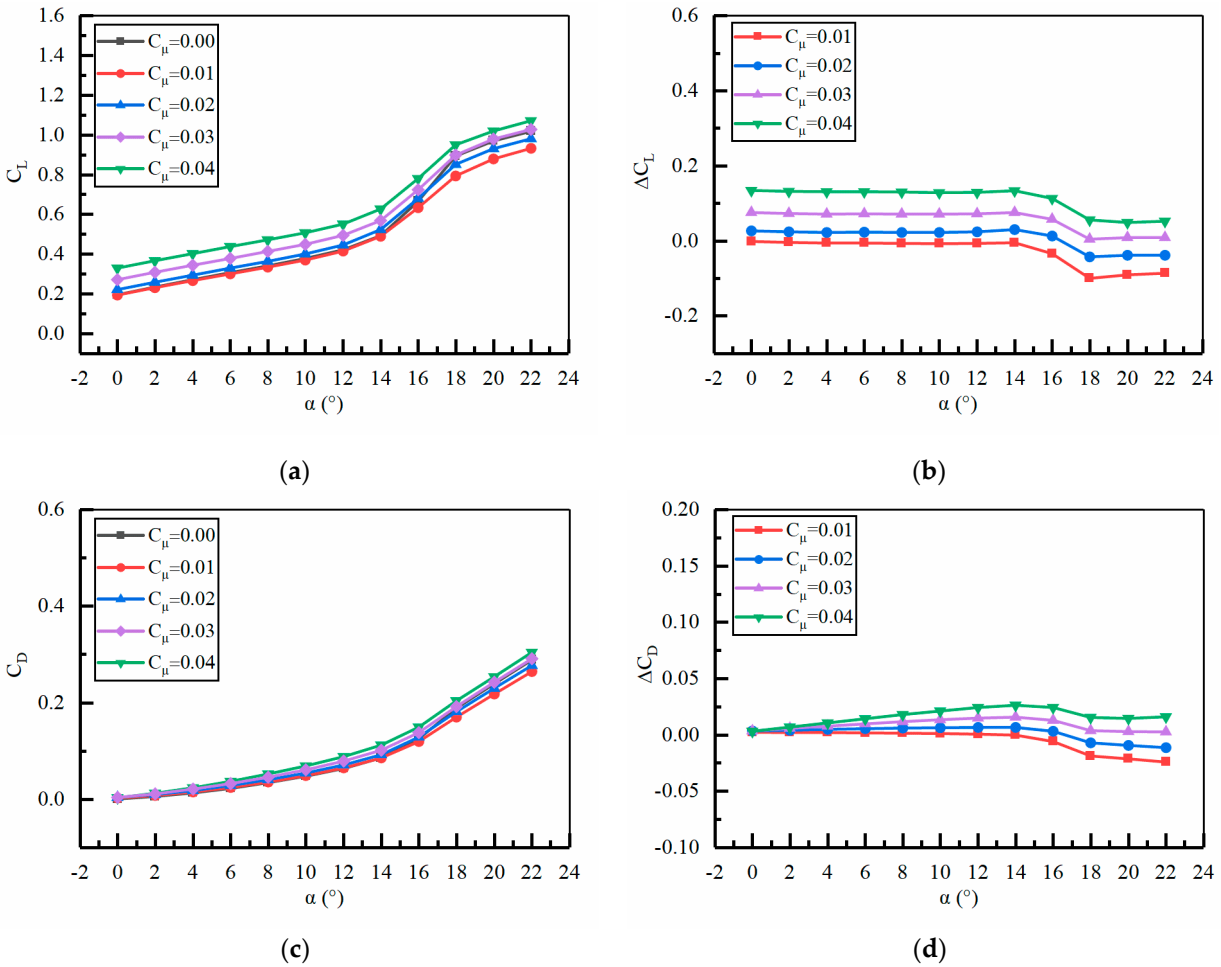

(**a**) (**b**)

(**c**) (**d**)

Figure 6. The improvement effect of momentum coefficient on the aerodynamic performance under 20% leading edge jet conditions. (**a**) Lift coefficient; (**b**) growth value of lift coefficient; (**c**) drag coefficient; (**d**) growth value of drag coefficient.

4.2. The Improvement Effect of Jet Hole Height on Aerodynamic Performance

The improvement effect of jet hole height on the aerodynamic performance of ducted tail wing is studied. The calculation state is selected as Reynolds number Re = 8.43 × 10^5, flow velocity Ma = 0.15, jet hole height H_2 = 0.00%c/0.25%c/0.35%c/0.45%c, jet angle $\theta_2 = 0^\circ$, jet hole position L_1 = 100%c, jet momentum coefficients C_μ = 0.02 and 0.04.

As shown in Figure 7a, when the jet hole position L_1 = 100%c and the jet momentum coefficient C_μ = 0.02, with the increase of H_2, the fluid velocity injected into the flow field per unit time decreases, and the airflow disturbance of the ducted tail decreases, resulting in a weakened lift coefficient C_L enhancement effect of the ducted tail. As shown in Figure 7b, within the angle of attack range of 0°–22°, with C_μ = 0.00 and no jet state as the reference, C_μ = 0.02, H_2 = 0.25%c, the average of ΔC_L is 0.196; When C_μ = 0.02 and H_2 = 0.35%c, the average of ΔC_L is 0.192; When C_μ = 0.02 and H_2 = 0.45%c, the average of ΔC_L is 0.145; It can be seen that as H_2 increases, the increase in lift coefficient C_L decreases. As shown in Figure 7c, with the increase of H_2, the airflow disturbance at the trailing edge of the ducted tail decreases, resulting in a weakened effect of improving the drag coefficient C_D of the ducted tail. As shown in Figure 7d, overall, the change in jet hole height has little effect on the drag coefficient C_D of the jet ducted tail wing.

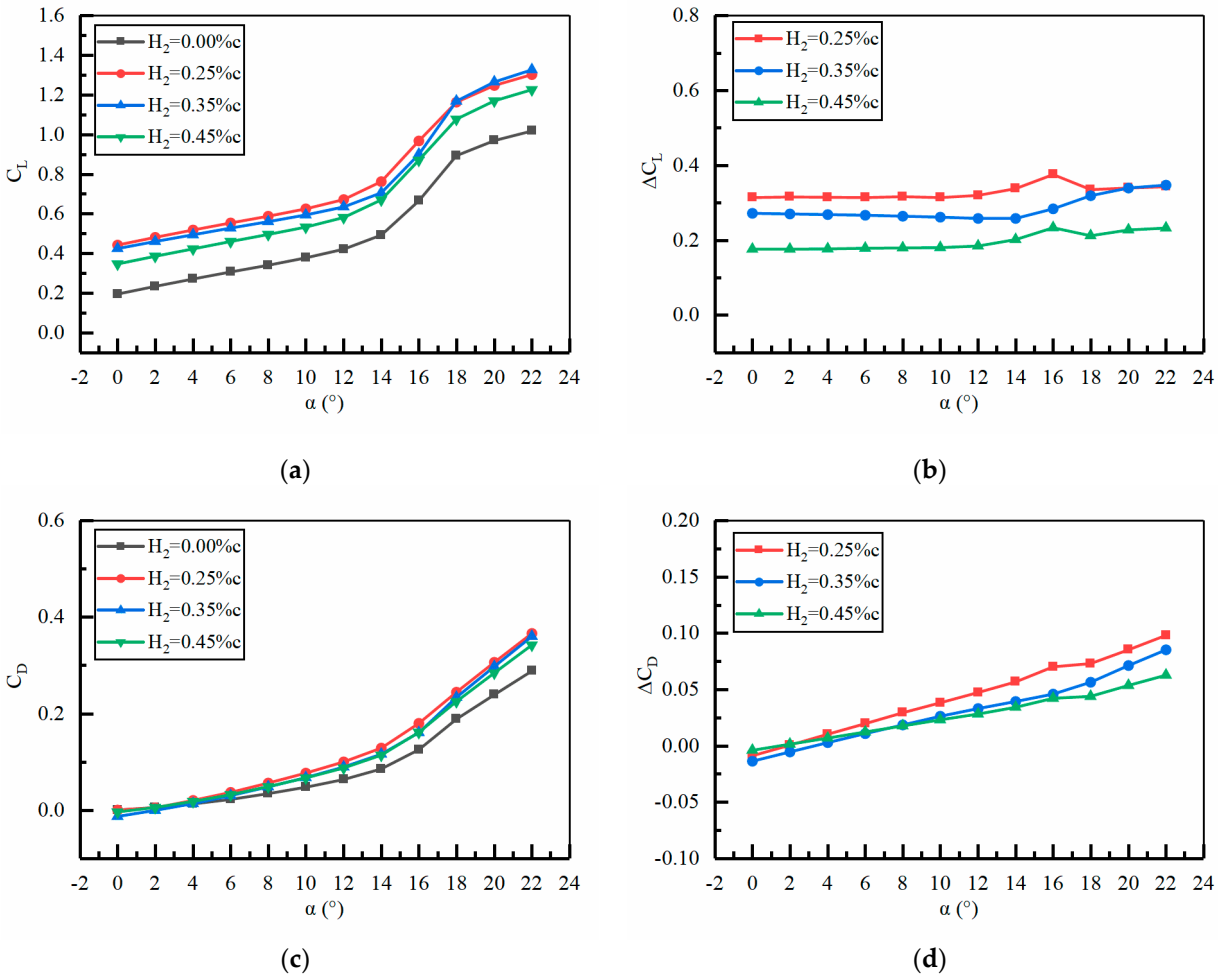

Figure 7. The improvement effect of jet hole height on aerodynamic performance in the state of momentum coefficient 0.02. (**a**) Lift coefficient; (**b**) growth value of lift coefficient; (**c**) drag coefficient; (**d**) growth value of drag coefficient.

Under the same conditions, when the jet momentum coefficient C_μ = 0.04, as shown in Figure 8a, with the increase of H_2, the effect of the change in jet hole height on the lift coefficient of the ducted tail is more significant compared with the momentum coefficient

C_μ = 0.02. As shown in Figure 8b, within the attack angle range of 0°–22 °, with C_μ = 0.00 and no jet state as the reference, C_μ = 0.04, H_2 = 0.25%c, the average of ΔC_L is 0.262; When C_μ = 0.04 and H_2 = 0.35%c, the average of ΔC_L is 0.239; When C_μ = 0.04 and H_2 = 0.45%c, the average of ΔC_L is 0.171; It can be seen that as the height of the jet hole increases, the growth rate of the lift coefficient C_L significantly decreases. As shown in Figure 8c, with the increase of H_2, the airflow disturbance at the trailing edge of the ducted tail decreases, resulting in a weakened effect of improving the drag coefficient C_D of the ducted tail. As shown in Figure 8d, compared with Figure 7d, overall, the change in jet hole height has a more significant impact on the drag coefficient C_D of the ducted tail wing. Overall, as the momentum coefficient C_μ of the jet increases, the effect of H_2 variation on the aerodynamic performance of the ducted tail becomes more significant.

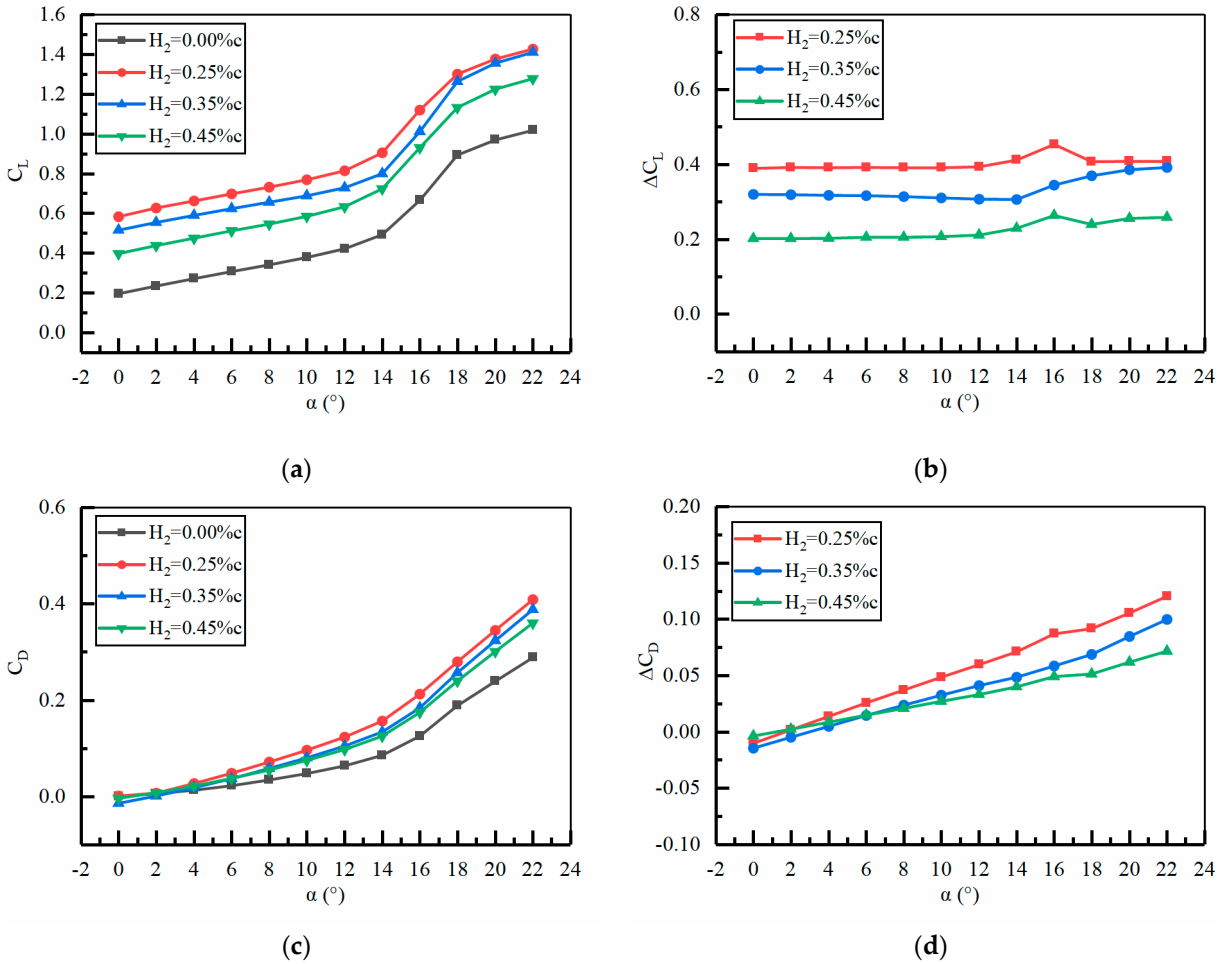

Figure 8. The improvement effect of jet hole height on aerodynamic performance in the state of momentum coefficient 0.04. (**a**) Lift coefficient; (**b**) growth value of lift coefficient; (**c**) drag coefficient; (**d**) growth value of drag coefficient.

4.3. The Improvement Effect of Jet Hole Position on Aerodynamic Performance

The calculation state selects Reynolds number Re = 8.43 × 10^5, flow velocity Ma = 0.15, jet hole height H_2 = 0.25%c, jet angle θ_2= 0°, jet momentum coefficient C_μ = 0.04, jet hole position L_1 = 20%c/40%c/60%c/80%c/100%c, and analyzes the improvement effect of different jet hole positions on the aerodynamic performance of the ducted tail wing.

As shown in Figure 9a, when the jet angle is 0° and the jet momentum coefficient C_μ is 0.04, as the distance L_1 between the jet hole and the leading edge increases, the lift coefficient C_L of the ducted tail wing is enhanced. Among them, L_1 = 100%c (the jet hole is located at the trailing edge of the tail wing) is most conducive to lift enhancement. As

shown in Figure 9b, within the attack angle range of 0°~22 °, with C_μ = 0.00 and no jet state as the reference, C_μ = 0.04, L_1 = 20%c, the average of ΔC_L is 0.154; When C_μ = 0.04 and L_1 = 40%c, the average of ΔC_L is 0.185; When C_μ = 0.04 and L_1 = 60%c, the average growth value of ΔC_L is 0.192; When C_μ = 0.04 and L_1 = 80%c, the average of ΔC_L is 0.225; When C_μ = 0.04 and L_1 = 100%c, the average of ΔC_L is 0.403. We can find that as L_1 increases, the increase in lift coefficient C_L also increases, especially when L_1 = 100%c, which is most conducive to lift enhancement. As shown in Figure 9c, as L_1 increases, the drag coefficient C_D of the ducted tail also increases. As shown in Figure 9d, overall, the change in L_1 has little effect on the drag coefficient C_D of the ducted tail wing. However, when the jet hole position L_1 = 100%c, the drag coefficient of the tail wing also significantly increases.

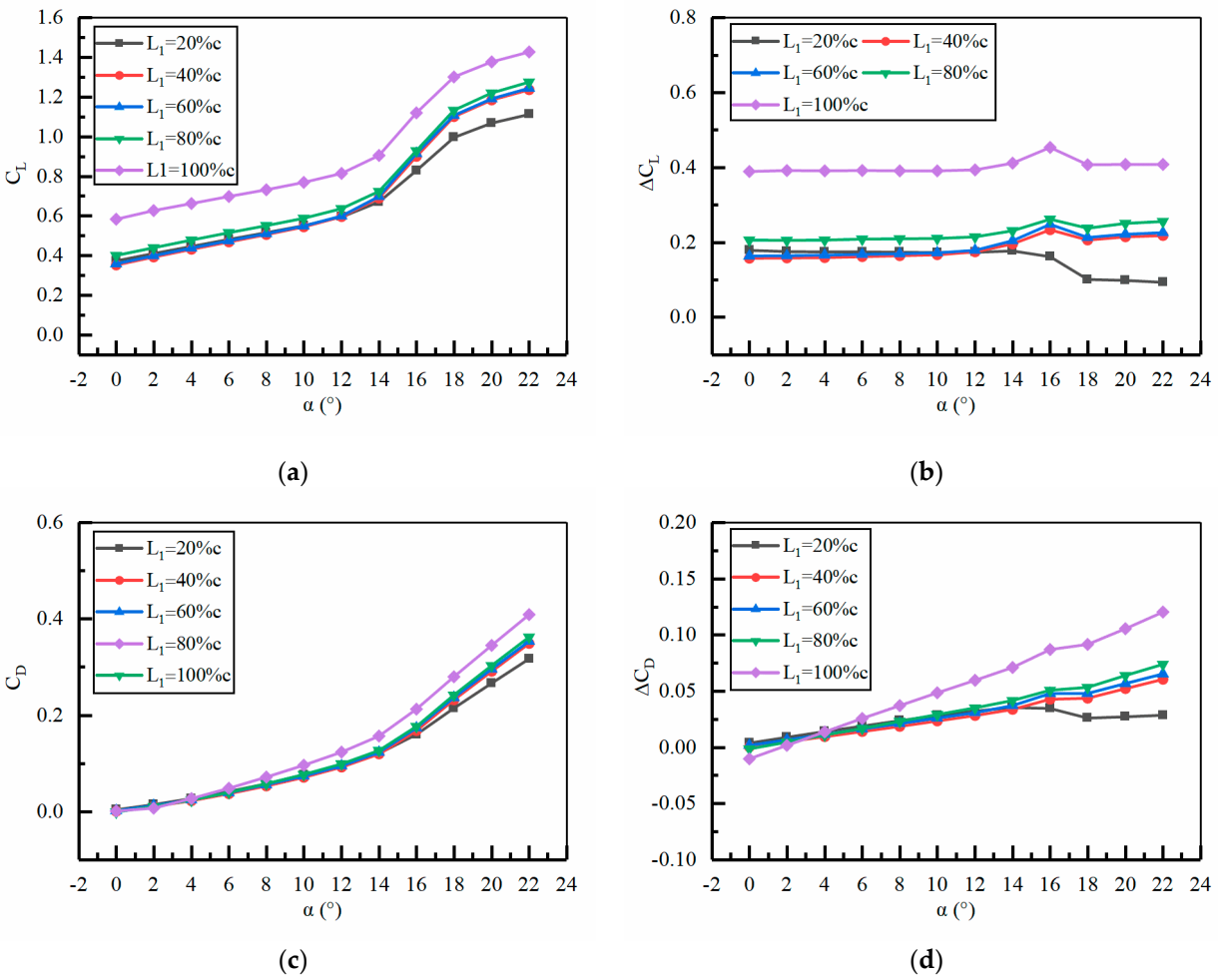

Figure 9. The improvement effect of jet hole position on aerodynamic performance at a jet angle of 0 ° and momentum coefficient of 0.04. (**a**) Lift coefficient; (**b**) growth value of lift coefficient; (**c**) drag coefficient; (**d**) growth value of drag coefficient.

Under the same conditions, when the jet angle is 10° and the jet momentum coefficient C_μ is 0.04, as shown in Figure 10a, the improvement effect of the jet hole position on the lift coefficient C_L decreases with the increase of the jet hole position L_1. As shown in Figure 10b, within the attack angle range of 0–22°, with C_μ = 0.00 and no jet state as the reference, when C_μ = 0.04 and L_1 = 20%c, the average of ΔC_L is 0.110; When C_μ = 0.04 and L_1 = 40%c, the average of ΔC_L is 0.175; When C_μ = 0.04 and L_1 = 60%c, the average of ΔC_L is 0.181; When C_μ = 0.04 and L_1 = 80%c, the average of ΔC_L is 0.205; When C_μ = 0.04 and L_1 = 100%c, the average of ΔC_L is 0.329. We find that as L_1 increases, the increase in lift coefficient C_L also increases, especially when L_1 = 100%c, which is most conducive to lift enhancement. As shown in Figure 10c, with the increase of L_1, the drag coefficient C_D of the ducted tail

increases. As shown in Figure 10d, compared with Figure 9d, overall, the effect of changes in the position of the jet holes on the drag coefficient C_D of the tail is weakened. Overall, when L_1 = 100%c, it is most beneficial for the ducted tail to increase lift and reduce drag.

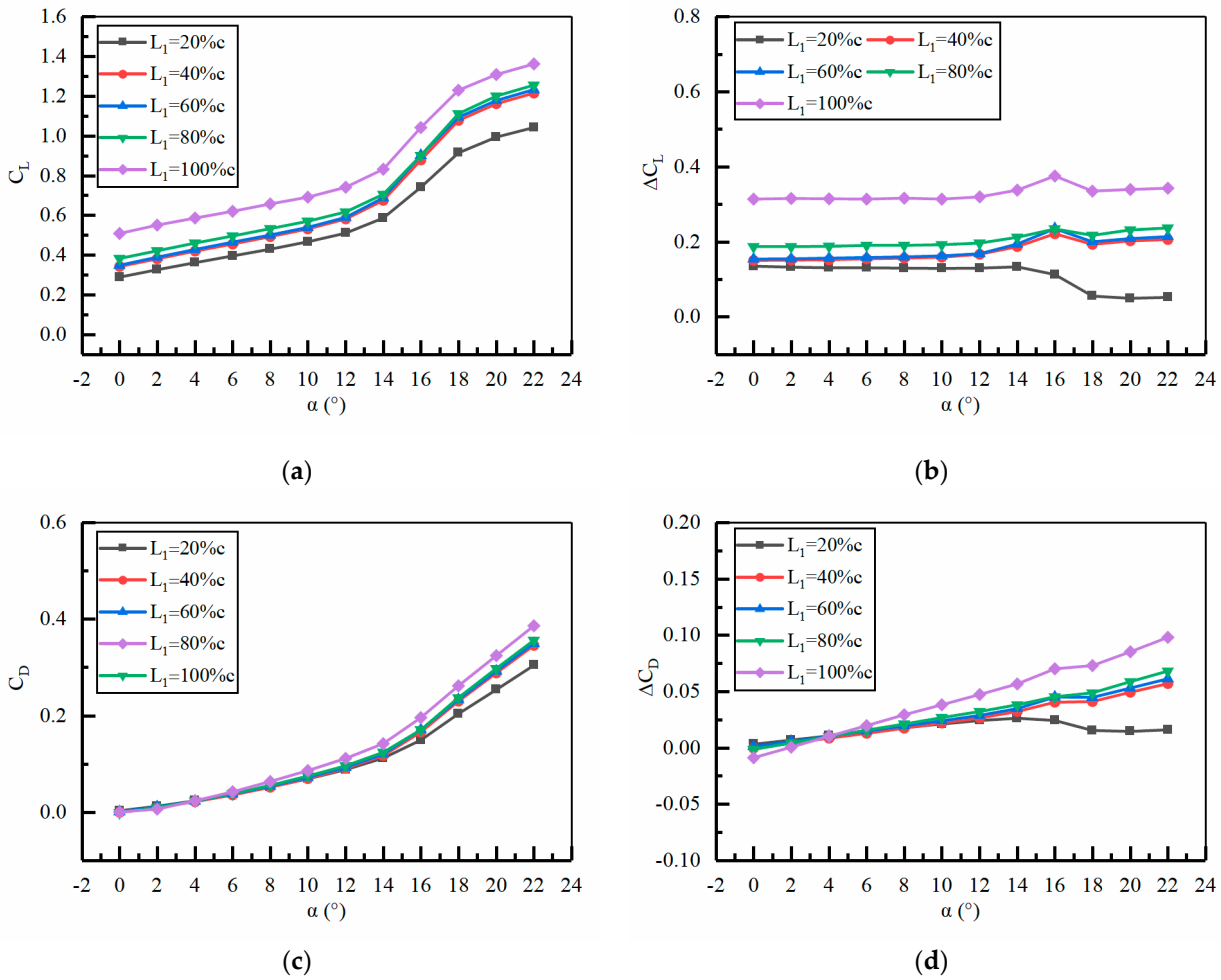

Figure 10. The improvement effect of jet hole position on aerodynamic performance at a jet angle of 10 ° and momentum coefficient of 0.04. (**a**) Lift coefficient; (**b**) growth value of lift coefficient; (**c**) drag coefficient; (**d**) growth value of drag coefficient.

4.4. The Improvement Effect of Jet Angle on Aerodynamic Performance

The calculation state is selected as Reynolds number Re = 8.43 × 10^5, flow velocity Ma = 0.15, jet hole height H_2 = 0.25%c, jet hole position L_1 = 20%c/40%c, jet momentum coefficient C_μ = 0.04. The influence of jet angles θ_1 = 0°, 10°, 20°, and 30° on the aerodynamic performance of ducted tail is analyzed.

As shown in Figure 11a, when L_1 = 20%c and the jet momentum coefficient C_μ = 0.04, as the jet angle θ_1 increases, the lift coefficient C_L of the ducted tail decreases. As shown in Figure 11b, within the attack angle range of 0°–22°, with C_μ = 0.00 and no jet state as the reference, when C_μ = 0.04 and θ_1 = 0°, the average of ΔC_L is 0.155; When C_μ = 0.04 and θ_1 = 10°, the average of ΔC_L is 0.110; When C_μ = 0.04 and θ_1 = 20°, the average of ΔC_L is 0.073; When C_μ = 0.04 and θ_1 = 30°, the average of ΔC_L is 0.063. It can be seen that as the jet angle increases, the increase in lift coefficient C_L decreases. As shown in Figure 11c, as the jet angle increases, the drag coefficient C_D of the ducted tail does not increase significantly. As shown in Figure 11d, overall, the increasing trend of drag coefficient C_D also decreases with the increase of the jet angle.

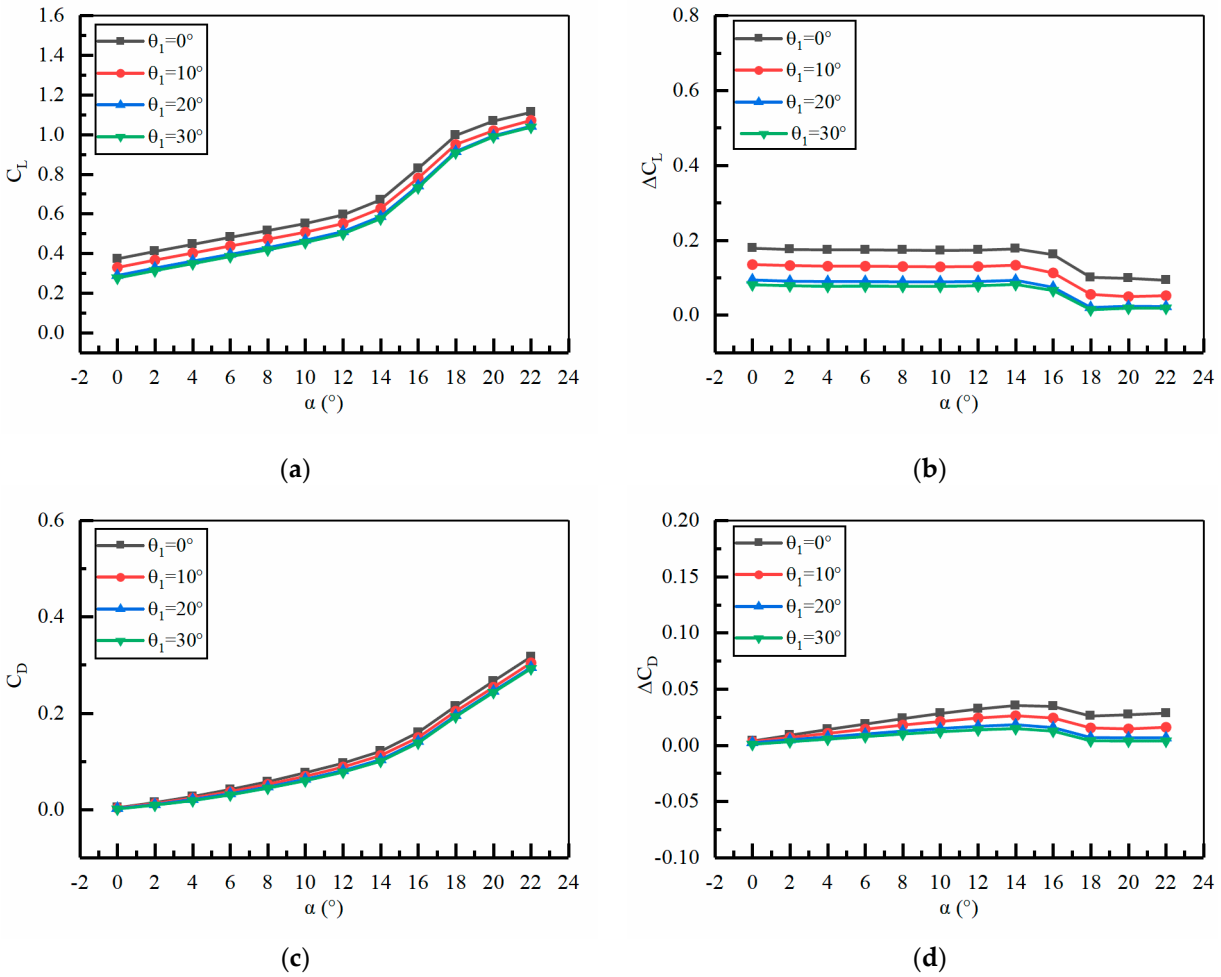

Figure 11. The improvement effect of jet angle on aerodynamic performance under the condition of leading edge 20% and momentum coefficient 0.04. (**a**) Lift coefficient; (**b**) growth value of lift coefficient; (**c**) drag coefficient; (**d**) growth value of drag coefficient.

As shown in Figure 12a, when L_1 = 40%c and the jet momentum coefficient C_μ = 0.04, the lift coefficient C_L of the ducted tail does not change significantly with the increase of the jet angle θ_1. As shown in Figure 12b, within the angle of attack range of 0°–22°, with C_μ = 0.00 and no jet state as the reference, when C_μ = 0.04 and θ_1 = 0°, the average of ΔC_L is 0.185; When C_μ = 0.04 and θ_1 = 10°, the average of ΔC_L is 0.175; When C_μ = 0.04 and θ_1 = 20°, the average of ΔC_L is 0.169; When C_μ = 0.04 and θ_1 = 30°, the average of ΔC_L is 0.168. It can be seen that when L_1 = 40%c and the jet momentum coefficient C_μ = 0.04, the increase in lift coefficient C_L does not show significant changes with the increase of jet angle. As shown in Figure 12c, with the increase of jet angle, there is no significant change in the drag coefficient C_D of the ducted tail. As shown in Figure 12d, overall, as the jet angle increases, the increase in drag coefficient C_D is very small.

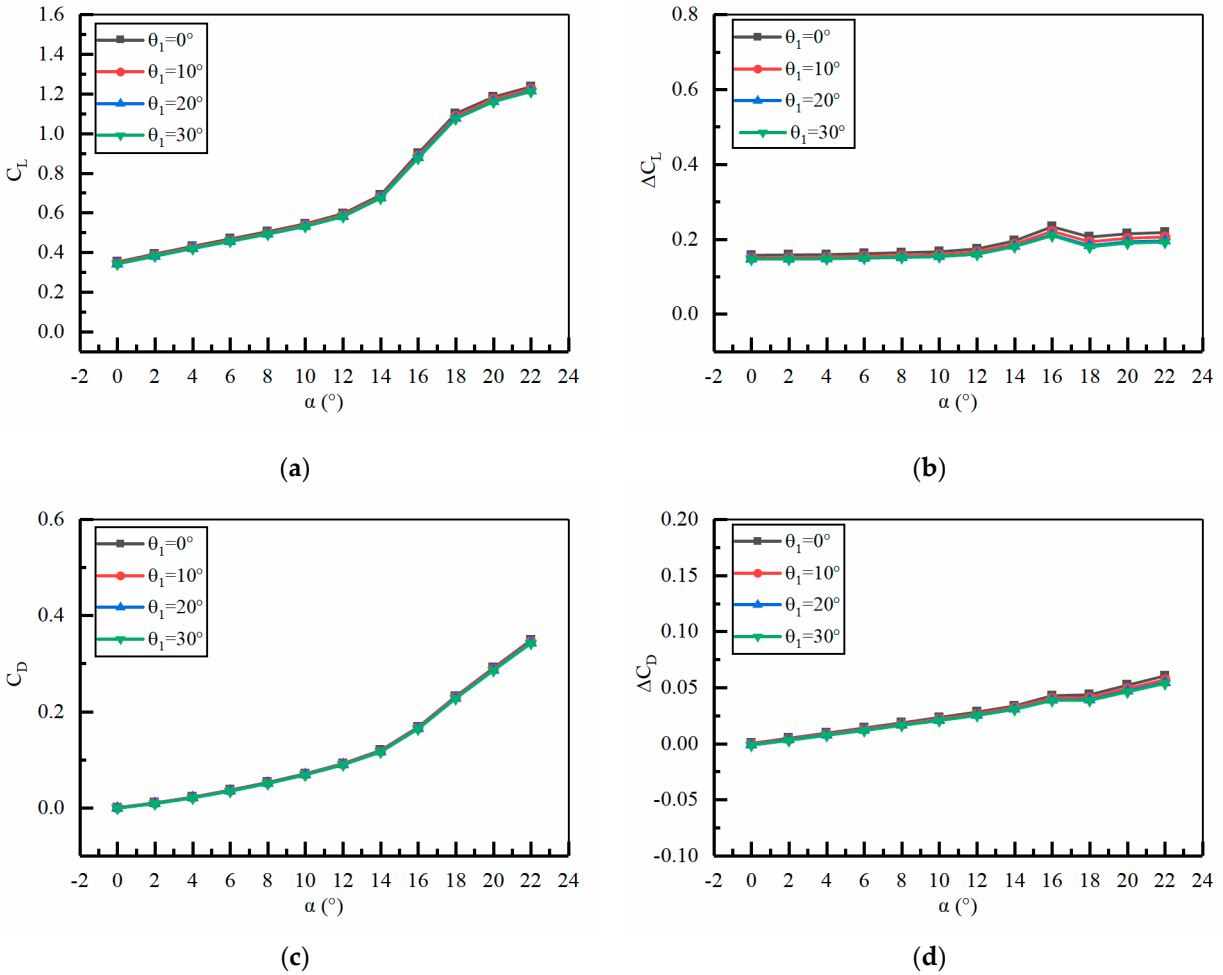

Figure 12. The improvement effect of jet angle on aerodynamic performance under the condition of leading edge 40% and momentum coefficient 0.04. (**a**) Lift coefficient; (**b**) growth value of lift coefficient; (**c**) drag coefficient; (**d**) growth value of drag coefficient.

4.5. Advantages and Principle Analysis of the Ducted Tail Wing

From the analysis in Sections 4.1–4.4, compared with jet hole height and jet angle, momentum coefficient and jet hole position are more effective in improving the aerodynamic performance of the ducted tail wing. When the jet hole height H_2 is 0.25%c, the jet angle is 0°, and L_1 is 100% c (trailing edge jet), the effect of increasing lift and reducing drag of the tail is relatively good with the increase of momentum coefficient.

Comparing the aerodynamic performance of ducted tail fins and traditional horizontal tail fins, the NACA0012 airfoil is selected for the traditional horizontal tail fin. In order to highlight the aerodynamic advantages of the ducted tail wing, the three-dimensional flow effect of the traditional tail wing is ignored, and its aerodynamic performance is simplified to that of the NACA0012 airfoil. As shown in Figure 13a, the lift coefficients of the ducted tail and NACA0012 airfoil are compared and analyzed under different jet conditions. It is found that the ducted tail can generate lift at 0° angle of attack so it can generate control force at low angles of attack. At the same time, it was found that the traditional NACA0012 airfoil began to stall after a 12° angle of attack, with a decrease in lift coefficient, which is not conducive to the control of the aircraft at high attack angles. However, the ducted tail does not enter the stall state after a 12° angle of attack and could provide momentum for aircraft control at high attack angles. As shown in Figure 13b, compared with the traditional NACA0012 airfoil, the ducted tail wing has a higher drag coefficient than the NACA0012 due to the blunting of the fillet at the trailing edge of the jet when the angle of attack is 0°~14°. However, as the angle of attack continues to increase, the traditional NACA0012

airfoil stalls, and the drag coefficient suddenly increases. However, the ducted tail does not stall. At jet momentum coefficients of 0.00 and 0.01, the drag coefficient is slightly lower than that of NACA0012.

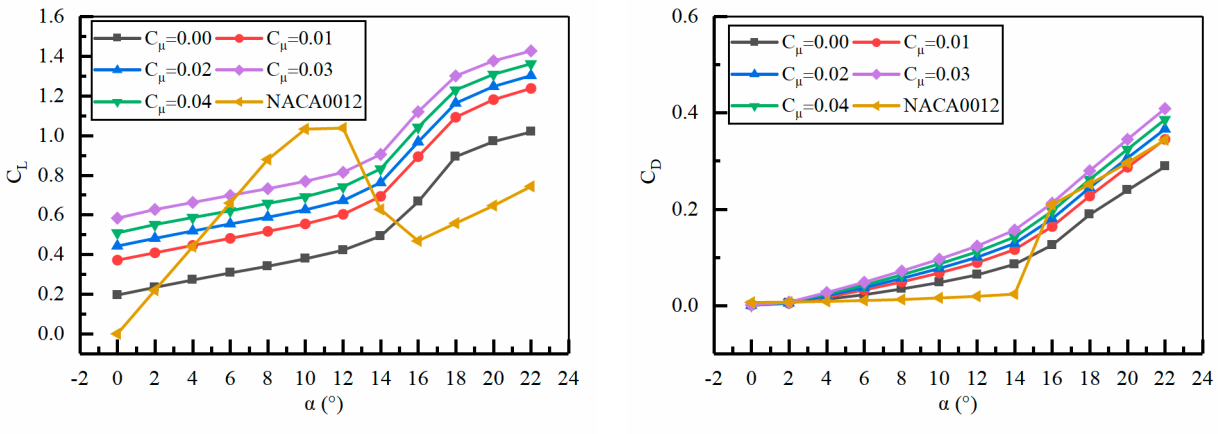

Figure 13. Comparison of lift and drag characteristics between the ducted tail and conventional tail. (**a**) Comparison of lift coefficients; (**b**) comparison of drag coefficients.

In order to analyze the reason why the ducted tail generates lift at a 0° attack angle and does not stall at high attack angles, we selected two states of 0° and 20° angles of attack and compared and analyzed the velocity and pressure cloud maps under the conditions of momentum coefficients of 0.01 and 0.04.

As shown in the velocity cloud maps of Figure 14a,b, at a 0° angle of attack, the airflow on the upper surface of the leading edge of the tail begins to accelerate after passing through the duct area formed by the tail and the fuselage, resulting in unequal pressure on the upper and lower surfaces of the tail. This is the main reason for the ducted tail wing generating lift at a 0° attack angle. As the C_μ increases, the airflow disturbance injected into the trailing edge of the ducted tail increases, and under the excitation of the Coanda effect, the lift coefficient of the tail further increases. As shown in Figure 14c,d, at a 20°attack angle, the induction at the tail of the fuselage causes the high attack angle airflow to deflect downward, resulting in the attack angle of the airflow flowing through the upper surface of the tail wing being less than 20°. Therefore, the ducted tail wing will not stall at an angle of attack of 20°. Due to the acceleration effect of the ducted wing, the airflow passing through the upper surface of the tail wing at a 20° angle of attack forms a high-speed zone, further enhancing the lift coefficient of the ducted tail wing. And as the momentum coefficient C_μ increases, the airflow disturbance injected into the trailing edge of the ducted tail increases, and under the excitation of the Coanda effect, the lift coefficient of the tail further increases.

Similarly, as shown in Figure 15a,b, due to the acceleration effect of the ducted effect on the surface airflow of the tail, there is a pressure difference between the upper and lower surfaces of the ducted tail at 0° angle of attack, further explaining the reason for the lift of the ducted tail at a 0° angle of attack. Moreover, as the momentum coefficient increases, the airflow disturbance injected into the trailing edge of the ducted tail increases. Under the excitation of the Coanda effect, there is a significant pressure difference between the upper and lower parts of the trailing edge of the tail, which is also the reason for the increase in the lift coefficient of the tail. As shown in Figure 15c,d, at a high angle of attack of 20°, due to the deflection effect of the tail of the fuselage on the high angle of attack airflow, the pressure difference between the upper and lower surfaces of the tail increases, and there is no sudden increase in pressure on the upper surface caused by the stall. Therefore, the lift coefficient of the ducted tail further increases.

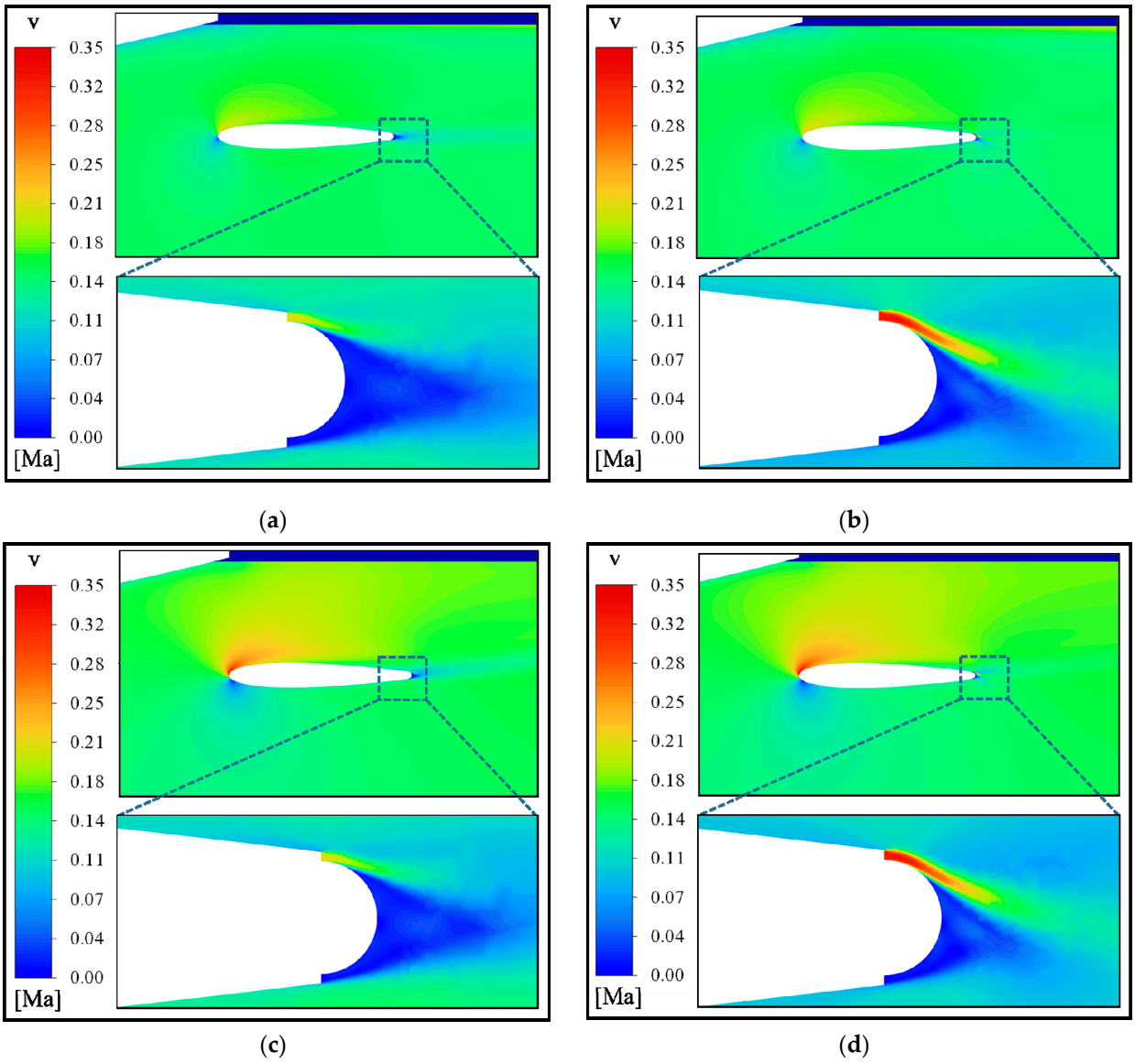

Figure 14. Cloud maps of ducted tail wing. (**a**) $C_\mu = 0.01, \alpha = 0°$ (**b**) $C_\mu = 0.04, \alpha = 0°$; (**c**) $C_\mu = 0.01, \alpha = 20°$; (**d**) $C_\mu = 0.04, \alpha = 20°$.

As shown in Figure 16, further comparison and analysis are conducted on the changes in pressure coefficients on the upper and lower surfaces of the ducted tail when the momentum coefficient changes. Two states of 0° and 20° angle of attack are selected to analyze the pressure coefficient difference of the ducted tail under different momentum coefficients. Through comparative analysis, taking the no-jet state $C_\mu = 0.00$ as a reference, it is found that as the momentum coefficient increases, the pressure coefficient difference at the trailing edge of the ducted tail increases rapidly. In addition, due to the induced effect of airflow, the pressure coefficient on the entire lower surface of the tail decreases, and the pressure difference with the upper surface increases, further improving the lift coefficient of the ducted tail.

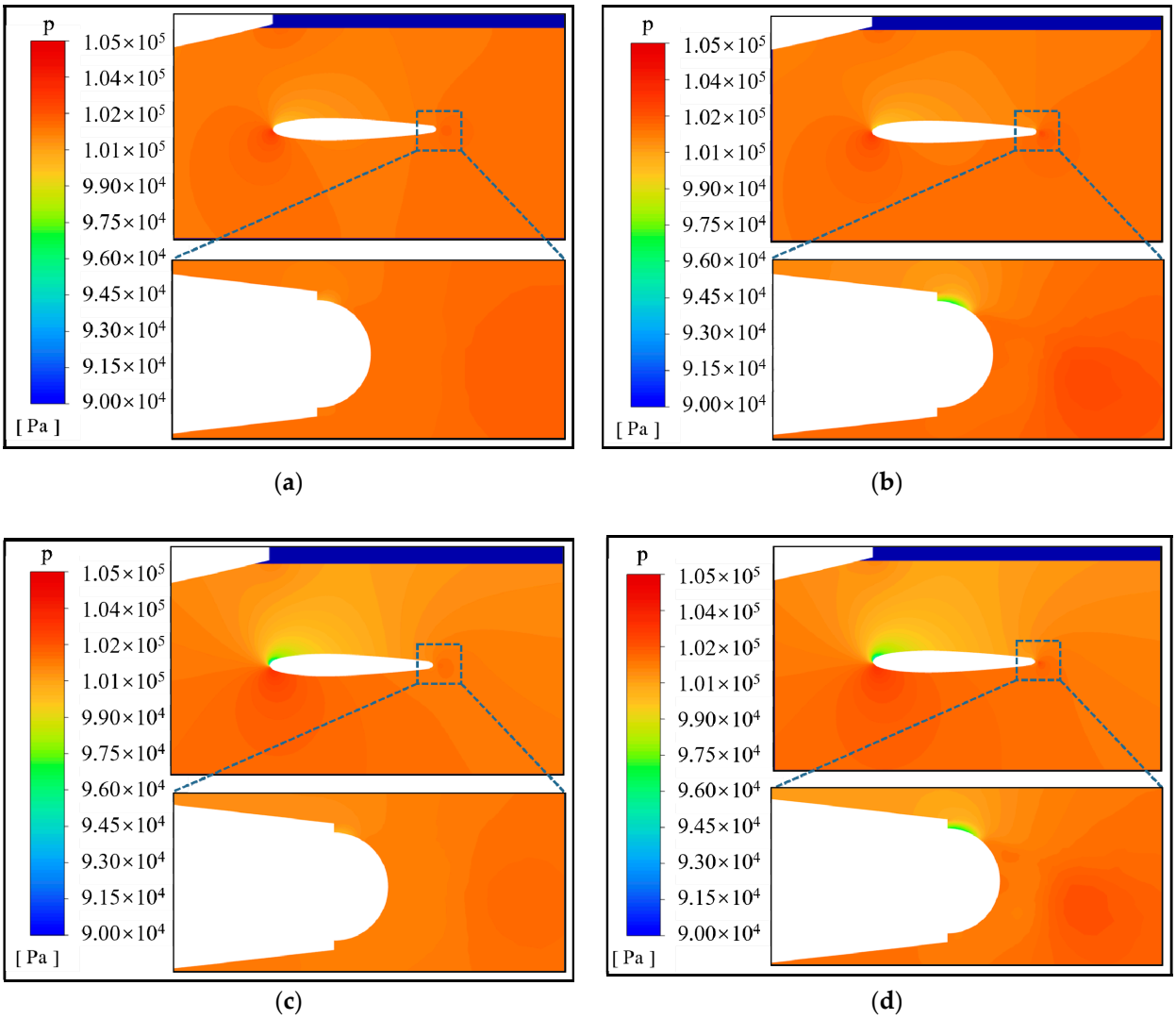

Figure 15. Pressure cloud maps for ducted tail wing. (**a**) $C_\mu = 0.01, \alpha = 0°$ (**b**) $C_\mu = 0.04, \alpha = 0°$; (**c**) $C_\mu = 0.01, \alpha = 20°$; (**d**) $C_\mu = 0.04, \alpha = 20°$.

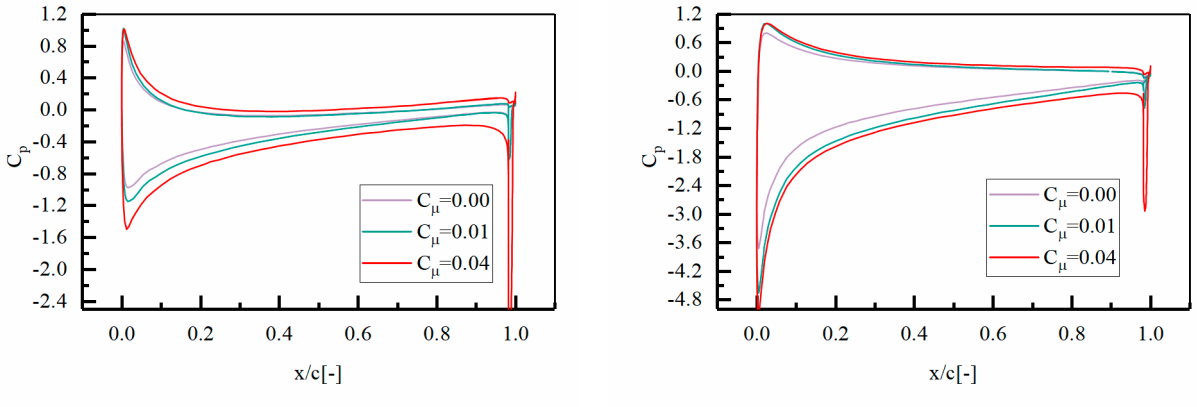

Figure 16. Comparison of pressure coefficients of ducted tail wing. (**a**) Comparison of pressure coefficients at $\alpha = 0°$ (**b**) comparison of pressure coefficients at $\alpha = 20°$.

5. Conclusions

This article takes the ducted tail of a certain box-type launch vehicle as the research object. The integrated nonfolding ducted tail proposed in this article can solve the problem of storing the tail in the launch box. Moreover, traditional mechanical control surfaces have been eliminated, and active jet control has been adopted to control the pitch direction of the flight attitude, which can improve the structural reliability of the tail wing. By studying the effects of parameters such as momentum coefficient, jet hole position, jet hole height, and jet angle on improving the aerodynamic performance of ducted tail wing, we obtain the following conclusion.

(1) The improvement effect of jet hole height and jet angle on the aerodynamic performance of ducted tail wing is relatively small. Through comparative analysis, it is found that under the conditions of jet hole height H_2 = 0.25%c and jet angle $\theta_1 = 0^\circ$, it is more conducive to improving the aerodynamic performance of the ducted tail wing.

(2) The momentum coefficient and jet hole position are the main factors affecting the aerodynamic performance of the ducted tail wing. Under the conditions of H_2 = 0.25%c, jet angle $\theta_1 = 0^\circ$, and L_1 = 100%c (jet hole located at the trailing edge of the tail wing), the improvement effect of the aerodynamic performance of the tail wing is relatively good as the momentum coefficient C_μ increases. At C_μ = 0.04, the average of ΔC_L is 0.403; When C_μ = 0.03, the average of ΔC_L is 0.329; When C_μ = 0.02, the average of ΔC_L is 0.262; When C_μ = 0.01, the average of ΔC_L is 0.191. When C_μ increases from 0.01 to 0.04, the average growth of ΔC_L can reach 110%.

(3) A comparative analysis is conducted on the aerodynamic performance of ducted tail wings and NACA0012 airfoils. It is found that the ducted tail can generate lift at a 0° angle of attack. In this way, under low angle of attack conditions, the ducted tail can generate control force without jet flow, which can save control energy. Compared with the NACA0012 airfoil, the ducted tail does not stall at angles of attack $\geq 12^\circ$ and can provide stable control momentum for the aircraft at high attack angles.

Author Contributions: Conceptualization, H.J.; Methodology S.H.; Validation, H.J. and. S.H.; Writing original draft preparation, H.J.; Supervision, H.J.; Visualization, H.Z. (Hong Zhou) and H.Z. (Huilong Zheng). All authors have read and agreed to the published version of the manuscript.

Funding: This research was funded by the National Key Laboratory of Science and Technology on Advanced Light-duty Gas-turbine (E31H890206).

Data Availability Statement: Due to the limitations of the Ethics Review Committee, these data cannot be made public to protect the privacy and confidential information of the subjects. The data presented in this study are available upon request from the corresponding author.

Acknowledgments: The authors would like to sincerely thank the relevant organizations and institutions for their support of this study.

Conflicts of Interest: The authors declare no conflicts of interest.

References

1. Anderson, J.D. *Fundamentals of Aerodynamics*; McGraw-Hill: New York, NY, USA, 2005.
2. Warsop, C.; Crowther, W.J. Fluidic Flow Control Effectors for Flight Control. *AIAA J.* **2018**, *56*, 3808–3824. [CrossRef]
3. Warsop, C.; Crowther, W. NATO AVT-239 Task Group: Flight Demonstration of Fluidic Flight Controls on the MAGMA Subscale Demonstrator Aircraft. In Proceedings of the AIAA Scitech 2019 Forum, San Diego, CA, USA, 7–11 January 2019.
4. Jones, G.S.; Joslin, R.D. *Applications of Circulation Control Technology*; Progress in Astronautics & Aeronautics; American Institute of Aeronautics and Astronautics: Reston, VA, USA, 2015.
5. Englar, R.J. Development of Circulation Control Technology for Powered-Lift STOL Aircraft. 1987. Available online: https://ntrs.nasa.gov/citations/19880008224 (accessed on 17 March 2024).
6. Frith, S.; Wood, N. Investigation of Dual Circulation Control Surfaces for Flight Control. In Proceedings of the Aiaa Flow Control Conference, Portland, OR, USA, 28 June–1 July 2015.

7. Fielding, J.; Lawson, C.; Martins-Pires, R.; Monterzino, G. Design, Build and Flight of The DEMON Demonstrator UAV. In Proceedings of the 11th AIAA Aviation Technology, Integration, and Operations (ATIO) Conference, Virginia Beach, VA, USA, 20–22 September 2011.
8. Hoholis, G.; Steijl, R.; Badcock, K. Circulation Control as a Roll Effector for Unmanned Combat Aerial Vehicles. *J. Aircr.* **2016**, *53*, 1875–1889. [CrossRef]
9. Xu, H.Y.; Qiao, C.L.; Yang, H.Q.; Ye, Z.Y. Active Circulation Control on the Blunt Trailing Edge Wind Turbine Airfoil. *AIAA J.* **2017**, *56*, 554–570. [CrossRef]
10. Xu, H.Y.; Dong, Q.L.; Qiao, C.L.; Ye, Z.Y. Flow Control over the Blunt Trailing Edge of Wind Turbine Airfoils Using Circulation Control. *Energies* **2018**, *11*, 619. [CrossRef]
11. Fu, Z.; Chu, Y.W.; Cai, Y.S.; Xu, H.Y.; Xu, Y. Numerical Investigation of Circulation Control Applied to Flapless Aircraft. *Aircr. Eng. Aerosp. Technol.* 2020, *ahead-of-print*. [CrossRef]
12. Visser, K.D.; Nelson, R.C.; Ng, T.T. A Flow Visualization and Aerodynamic Force Data Evaluation of Spanwise Blowing on Full and Half Span Delta Wings. In Proceedings of the 27th Aerospace Sciences Meeting, Reno, NV, USA, 9–12 January 1989.
13. Amitay, M.; Anders, S.G.; Parekh, D.E.; Washburn, A.E. Active Flow Control on the Stingray Uninhabited Air Vehicle: Transient Behaviour. *AIAA J.* **2004**, *42*, 2205–2215. [CrossRef]
14. Mahmood, G.; Smith, D. Proportional Aerodynamic Control on a UAV Model Using Synthetic Jets. In Proceedings of the 37th AIAA Fluid Dynamics Conference and Exhibit, Miami, FL, USA, 25–28 June 2007.
15. Englar, R.; Jones, G.; Allan, B.; Lin, J. 2-D Circulation Control Airfoil Benchmark Experiments Intended for CFD Code Validation. In Proceedings of the Aiaa Aerospace Sciences Meeting Including the New Horizons Forum & Aerospace Exposition, Orlando, FL, USA, 5–8 January 2009.
16. Jones, G.S.; Englar, R.J. Advances in Pneumatic-Controlled High-Lift Systems Through Pulsed Blowing. In Proceedings of the 21st AIAA Applied Aerodynamics Conference, Orlando, FL, USA, 23–26 June 2003.
17. Jones, G.S.; Viken, S.A.; Washburn, A.E.; Jenkins, L.N.; Cagle, C.M. An Active Flow Circulation Controlled Flap Concept for General Aviation Aircraft Applications. In Proceedings of the 1st AIAA Flow Control Conference, St. Louis, MI, USA, 24–26 June 2002.
18. Liu, Y.; Sankar, L.N.; Englar, R.; Ahuja, K.K.; Gaeta, R. Computational Evaluation of the Steady and Pulsed Jet Effects on the Performance of a Circulation Control Wing Section. In Proceedings of the 42nd AIAA Aerospace Sciences Meeting and Exhibit, Reno, NV, USA, 5–8 January 2003.
19. Feng, L.H.; Shi, T.Y.; Liu, Y.G. Lift Enhancement of an Airfoil and an Unmanned Aerial Vehicle by Plasma Gurney Flaps. *Aiaa J.* **2017**, *55*, 1622–1632. [CrossRef]
20. Itsariyapinyo, P.; Sharma, R.N. Large Eddy Simulation of a NACA0015 Circulation Control Airfoil Using Synthetic Jets. *Aerosp. Sci. Technol.* **2018**, *82–83*, 545–556. [CrossRef]
21. Blackwell, J.A. Aerodynamic Characteristics of an 11-Percent-Thick Symmetrical Supercritical Airfoil at Mach Numbers between 0.30 and 0.85. 1969. Available online: https://ntrs.nasa.gov/citations/19830002814 (accessed on 12 March 2024).